Updates on CYGNSS Ocean Surface Wind Validation in the Tropics

SHAKEEL ASHARAF,[a,b] DEREK J. POSSELT,[b] FAOZI SAID,[c,d] AND CHRISTOPHER S. RUF[e]

[a] *Joint Institute for Regional Earth System Science and Engineering, University of California, Los Angeles, Los Angeles, California*
[b] *Jet Propulsion Laboratory, California Institute of Technology, Pasadena, California*
[c] *NOAA/NESDIS/Center for Satellite Applications and Research, College Park, Maryland*
[d] *Global Science and Technology, Inc., Greenbelt, Maryland*
[e] *University of Michigan, Ann Arbor, Michigan*

(Manuscript received 17 November 2021, in final form 18 July 2022)

ABSTRACT: Global Navigation Satellite System Reflectometry (GNSS-R)-based wind retrieval techniques use the global positioning system (GPS) signals scattered from the ocean surface in the forward direction, and can potentially work in all weather conditions. An overview of recent progress made in the Cyclone Global Navigation Satellite System (CYGNSS) level-2 surface wind products is given. To this end, four publicly released CYGNSS surface wind products—Science Data Record (SDR) v2.1, SDR v3.0, Climate Data Record (CDR) v1.1, and science wind speed product NOAA v1.1—are validated quantitatively against high-quality data from tropical buoy arrays. The latest released CYGNSS wind products (e.g., CDR v1.1, SDR v3.0, NOAA v1.1), as compared with these tropical buoy data, significantly outperform the SDR v2.1. Moreover, the uncertainty among these products is found to be less than 2 m s^{-1} root-mean-squared difference, meeting the NASA science mission level-1 uncertainty requirement for wind speeds below 20 m s^{-1}. The quality of the CYGNSS wind is further assessed under different precipitation conditions in low winds, and in large-scale convective regions. Results show that the presence of rain appears to cause a slightly positive wind speed bias in all CYGNSS data. Nonetheless, the outcomes are encouraging for the recently released CYGNSS wind products in general, and for CYGNSS data in regions with precipitating deep convection. The overall comparison indicates a significant improvement in wind speed quality and sample size when going from the older version to any of the newer datasets.

KEYWORDS: Atmosphere; Ocean; Buoy observations; Microwave observations; Remote sensing; Satellite observations

1. Introduction

Scatterometer derived surface winds significantly contribute to scientific understanding of complex air–sea dynamics and relevant key phenomena, especially where in situ observations are sparse and/or challenging to obtain. It has successfully been demonstrated that satellites are capable of resolving fine-scale wind variations and related air–sea dynamics (Alpers and Brümmer 1994; Short et al. 2019). For instance, Short et al. (2019) examined offshore characteristics of the Maritime Continent's diurnal wind cycles using satellite scatterometer observations, and noticed that land–sea breezes typically propagate as gravity waves over 400 km offshore, generating mean wind differences of 1–5 m s^{-1}. Moreover, satellite scatterometer estimates of 10-m winds are used to assess the accuracies of near-surface wind fields (Chelton and Freilich 2005) in forecasts from operational weather forecast agencies such as the National Centers for Environmental Prediction (NCEP; Saha et al. 2014) and the European Centre for Medium-Range Weather Forecasts (ECMWF; Hersbach et al. 2020). Scatterometer winds are routinely assimilated into weather forecast models, and have been shown to result in improved forecast skill (Kobayashi et al. 2015; Rennie et al. 2021; Rennie and Isaksen 2020). Improvements have also been seen in the prediction of cyclone tracks and tropical convection (Li et al. 2020; Bhate et al. 2021).

While near-surface wind data from spaceborne scatterometers have proven to be a source of accurate information, their performance can be substantially affected by specific environmental conditions. For instance, most scatterometer data are attenuated in heavy rain due to their relatively high operating frequencies such as the Ku-band operated QuikSCAT, ScatSAT, and RapidSCAT. However, attenuation has much less of an effect at lower frequencies, e.g., L or S band. The NASA CYGNSS constellation consists of eight observatories with GNSS receivers, and provides L-band bistatic scatterometry data via a signal of opportunity, using the operational GPS constellation as transmitters. CYGNSS measurements are free from the Bragg resonance (Ruf et al. 2019b), and are thus sensitive to a broader range of the roughness spectrum that includes both capillary waves and swell (Zavorotny and Voronovich 2000). The measurements are less sensitive to rainfall intensity than C- or Ku-band scatterometers. The CYGNSS mission consists of a constellation of eight small spacecraft orbiting at a low altitude of ~500 km and 35° inclination angle. As a result, it provides ample data sampling over the whole tropics, which are effective in representing natural events such as hurricanes. A detailed description of the CYGNSS mission and spacecraft engineering characteristics

Supplemental information related to this paper is available at the Journals Online website: https://doi.org/10.1175/JTECH-D-21-0168.s1.

Corresponding author: Shakeel Asharaf, shakeel.asharaf@jpl.nasa.gov

DOI: 10.1175/JTECH-D-21-0168.1

are given in the CYGNSS handbook (Ruf et al. 2016) and in the article by Ruf et al. (2019b).

CYGNSS winds are derived from ocean surface forward scattering through a geophysical model function (GMF) that maps the CYGNSS normalized bistatic radar cross section (NBRCS; or so-called σ_0) to 10-m wind speed. In the retrieval process, wind data output from operational numerical weather prediction model data assimilation systems were used to generate the CYGNSS level-2 GMF (e.g., Ruf and Balasubramaniam 2019; Said et al. 2021). The estimated CYGNSS retrieval winds can thus be influenced by a variety of environmental and geophysical conditions, including data calibration and the details of the GMF. Recent advancements in the CYGNSS L2 wind speed estimates include better calibrated NBRCS thanks to the monitoring of the GPS transmit power using the CYGNSS zenith antenna (Wang et al. 2019), as well as the use of a trackwise NBRCS bias correction to help address lingering calibration issues (Said et al. 2019). In fact, the latter has been incorporated in both the CDR data series (v1.0 and v1.1) and the NOAA v1.1 wind products. With the advancements made to the CYGNSS products over the previously released Science Data Record (SDR) v2.1, it is therefore important to assess the performance of these newly derived wind speed estimates. In this paper, our aim is to document the recent progress made in the publicly released CYGNSS data for the science and applications user communities. Quantitatively, the wind speeds observed by CYGNSS are evaluated using a high-quality set of tropical moored buoy arrays. Furthermore, the performance of CYGNSS in different oceanic regimes, under various large-scale convective phenomenon, and in buoy measured rain conditions are assessed in this study.

2. Data and validation approach

This study incorporates four publicly available CYGNSS level-2 wind products—SDR v2.1 and v3.0, CDR v1.1, and NOAA v1.1. Each data product provides the time-stamped and spatially averaged wind speed at 25-km effective resolution inferred from the Delay Doppler Mapping (DDM) instrument mounted on the CYGNSS spacecraft. All data versions, except NOAA v1.1, report a 25-km wind speed sample every ~6 km along each CYGNSS track. The NOAA v1.1 product, on the other hand, reports nonoverlapping adjacent 25-km wind speed samples along each CYGNSS track (i.e., wind speed samples are 25 km apart). While the DDM sampling frequency is 2 Hz (2 samples per second post–July 2019, giving ~3–4-km spatial distance between samples on the surface; before that it was 1 Hz ~6–8 km), the time difference between two consecutive wind speed samples is reported to be about 4–5 and ~1 s for the NOAA and the remaining (SDR v2.1, SDR v3.0, CDR v1.1) CYGNSS products, respectively. A brief description of each of the datasets as follows.

a. SDR v2.1

CYGNSS level-2 SDR version 2.1 (i.e., SDR v2.1) fully developed sea (FDS) surface winds were obtained from the PO.DAAC data web portal (CYGNSS 2018). The CYGNSS level-2 empirical GMF model used the closest 10-m ERA-Interim and GDAS Blended Sea Winds matchup to CYGNSS L2 wind speed sample (Ruf and Balasubramaniam 2019). The blended dataset was ocean surface vector winds on a global 0.25°, 6-hourly grid, which was used to generate the GMF at different wind ranges. More details about the algorithm can be found in the level-2 Wind Speed Retrieval algorithm theoretical basis document (Clarizia et al. 2018). The radiated power generated by GPS Block type IIF GPS spacecrafts was found to fluctuate significantly, and at times it was difficult or impossible to predict or detect. This led to a high level of uncertainty in CYGNSS winds derived from reflections from the GPS Block type IIF transmitters. Version 2.1 calibration did not apply a correction to fix this power fluctuation issue, and therefore in this version, the Block type IIF samples were excluded from the wind speed retrievals (Ruf et al. 2019b). In addition, the data points that have a range corrected gain (RCG) value less than 3 (unit: 1×10^{-27} dBi m^{-4}) were flagged and excluded from our analysis. The reason the RCGs were used as the quality control is the fact that smaller RCGs are often correlated with a high incidence angle, leading to a higher degree of uncertainty in the wind estimates (Ruf et al. 2016). In our current analysis, we have found that the statistics improve (RMSD by ~2.5% against the buoy winds) using the applied RCG thresholds in the SDR v2.1, despite a 4%–5% reduction in sample size.

b. SDR v3.0

Version 3.0 (CYGNSS 2020) is the successor of v2.1 in the SDR series. The major change involved incorporation of the tracking of direct signal strength using the zenith antenna which allows for real-time monitoring of the variations in GPS transmit power. This allows v3.0 to be more accurately calibrated than v2.1. Note that, prior to August 2018, each zenith antenna used automatic gain control. As such, no direct calibration is possible prior to August 2018, and v3.0 data are only available after this time. The real-time transmit power monitoring and correction implemented in level 1 v3.0 data allow Block II-F signals to be used. This provides a better estimation of the σ_0, which is then used with an updated GMF for the wind speed retrieval. Also, in this product version, measurements over the entire globe are matched up with coincident 10-m referenced ocean surface wind speeds provided by MERRA-2 data (Gelaro et al. 2017) that were used to generate the GMF.

c. CDR v1.1

Version 1.1 CDR (CYGNSS 2021) is the latest climate-quality release of the CYGNSS wind speed product, and is derived from the CYGNSS v3.0 level 1 data. The FDS level-2 wind speeds are derived using the same GMF as SDR v3.0 to map the observables into wind speed that are empirically derived from large populations of near-coincident matchups between on-orbit measurements by CYGNSS and an independent estimate of the MERRA-2 wind speed. Similar to Said et al. (2019), a trackwise correction algorithm is implemented, this time using MERRA-2 wind as ancillary model wind data. The trackwise correction accounts for

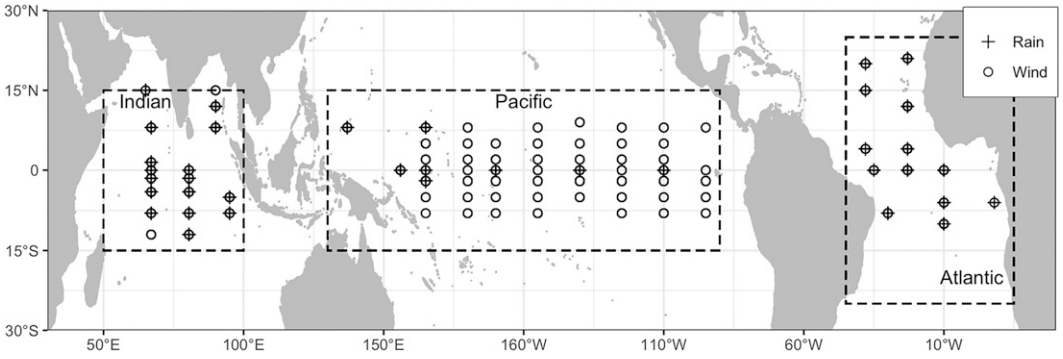

FIG. 1. The collocated (with CYGNSS SDR v2.1 from 1 Aug 2018 to 28 Feb 2021) tropical moored-buoy array: Prediction and Research Moored Array in the Tropical Atlantic (PIRATA), Research Moored Array for African–Asian–Australian Monsoon Analysis and Prediction (RAMA), and Tropical Atmosphere Ocean (TAO)/Triangle Transocean Buoy Network (TRITON) for winds (circles) and rainfall (plus signs). More details on the tropical buoys are given on the NOAA/PMEL website (www.pmel.noaa.gov/gtmba/mission).

any remaining transmit power level fluctuation of the GPS signals measured by the CYGNSS bistatic radar receivers that was not addressed in the v3.0 calibration routine as well as other possible residual calibration errors.

d. NOAA v1.1

This dataset (SOCD 2020) corresponds to the second science-quality release produced by NOAA/NESDIS, derived from SDR v2.1 NBRCS, using a geophysical model function dependent on both the wind speed and significant wave height, as well as the incidence angle of the specular reflection. Additionally, as part of the wind speed retrieval process, a trackwise debiasing algorithm is implemented on a track-by-track basis in order to remove the unwanted intersatellite biases including "inter-GPS block type" related biases [see Said et al. (2021) for more details]. Since CYGNSS NBRCS can be affected by the presence of swell, particularly in the low wind speed regime, the NOAA GMF takes into account the impact of the significant wave height in order to properly identify the contribution of the local wind to CYGNSS NBRCS.

e. Reference data

Following Asharaf et al. (2021), hourly averaged surface wind and rain observations from the tropical moored buoy arrays Prediction and Research Moored Array in the Tropical Atlantic (PIRATA; Bourlès et al. 2008), Research Moored Array for African–Asian–Australian Monsoon Analysis and Prediction (RAMA; McPhaden et al. 2009), and Tropical Atmosphere Ocean (TAO; McPhaden et al. 1998)/Triangle Transocean Buoy Network (TRITON) were processed and employed as reference data for the CYGNSS wind validation (Fig. 1).

f. Collocation method

CYGNSS derived ocean surface winds, from the time periods listed in Table 1 and the following figures, were validated against the ocean buoys. It is important to note that the SDR v2.1, SDR v3.0, and CDR v1.1 each provide two wind speed products called Young Sea Limited Fetch (YSLF) and Fully Developed Sea (FDS), whereas NOAA v1.1 provides a single wind speed product adapted for all wind conditions. In the case of the SDR v2.1, SDR v3.0, and CDR v1.1, the FDS wind product was selected for our study since it assumes the sea state is in equilibrium with the sea wind speed. Quality control (QC) flags were applied for the CDR v1.1, SDR v3.0, and NOAA v1.1 wind data, which were screened by discarding any records that were flagged as fatal or poor quality (see the QC-flags header description in the data). In this analysis, the daily GPS data were used to track a precise position of buoys over time.

CYGNSS winds were considered within 25 km and ±30 min of buoy locations and times, which were collocated by an inverse-distance-weighting (IDW) scheme that accounts for both the space and time between the measurements (Boutin and Etcheto 1990; Asharaf et al. 2021). It is likely that multiple CYGNSS specular points fall near a buoy location within the 25 km and ±30 min. Our collocation approach includes all of the specular points along the specular point track that both meet the spatial and temporal threshold criteria for the CYGNSS and buoy matchup. The calculation of weight in the applied IDW method is similar to the frozen turbulence concept as described by May and Bourassa (2011).

CYGNSS winds are reported at 10-m height. To perform a fair comparison, buoy winds were adjusted to 10-m height following Monin–Obukhov similarity theory using the Coupled Ocean–Atmosphere Response Experiment (COARE) version 3.6 (Edson et al. 2013; Fairall et al. 2003) algorithm. Moreover, the buoy winds were converted to equivalent neutral winds (U_{10n}) by removing the stability effects since satellite winds are derived from the radar signals that are uniquely related to wind stress rather than wind speeds (Liu 1984). It is important to mention here that the SDR v2.1 was derived from a GMF which incorporated GDAS blended sea winds. These blended winds are closer to U_{10n}. Therefore, we used the buoy U_{10n} wind for the SDR v2.1 comparison. However, the newer CYGNSS wind products differ in training data (real wind—e.g., CDR v1.1, SDR v3.0 used MERRA-2 reanalysis and NOAA

TABLE 1. Global and regional summary of statistical parameters [mean bias, RMSD, and correlation coefficient (Corr.) of wind speed between CYGNSS and buoy at different buoy measured wind ranges. *N* is the matchup sample size. All CYGNSS data cover the period from 1 Aug 2018 to 28 Feb 2021.

		Buoy wind range below 20 m s^{-1}											
		Low (wind $<$ 5 m s^{-1})				Moderate (5 $\leq$ wind $\leq$ 12 m s^{-1})				High (wind $>$ 12 m s^{-1})			
Coverage	CYGNSS product	*N*	Bias	RMSD	Corr.	*N*	Bias	RMSD	Corr.	*N*	Bias	RMSD	Corr.
Global	SDR v2.1	6412	0.87	2.30	0.5	14881	1.65	3.36	0.44	168	−0.58	3.01	0.19
	SDR v3.0	8030	0.08	1.26	0.6	16586	−0.82	1.88	0.5	185	−4.07	4.80	0.09
	CDR v1.1	6308	0.19	1.16	0.57	14145	−0.75	1.67	0.6	157	−3.22	4.09	0.03
	NOAA v1.1	7860	0.14	1.15	0.66	16346	−0.2	1.2	0.74	165	−1.86	3.07	0.12
Indian	SDR v2.1	2317	0.64	2.25	0.47	3603	1.41	3.19	0.50	109	−0.38	2.95	0.21
	SDR v3.0	2830	−0.05	1.24	0.61	3779	−1.09	2.06	0.56	121	−3.77	4.44	0.18
	CDR v1.1	2203	0.12	1.22	0.54	3244	−0.89	1.91	0.62	104	−2.99	3.64	0.11
	NOAA v1.1	2860	−0.02	1.12	0.67	3646	−0.48	1.38	0.76	103	−1.70	2.63	0.24
Pacific	SDR v2.1	3467	1.04	2.37	0.51	8383	1.87	3.49	0.43	33	−0.59	2.65	−0.10
	SDR v3.0	4395	0.14	1.29	0.59	9519	−0.74	1.84	0.47	42	−4.63	5.64	−0.21
	CDR v1.1	3418	0.25	1.14	0.59	8025	−0.64	1.58	0.59	32	−3.67	5.22	−0.24
	NOAA v1.1	4152	0.26	1.18	0.66	9251	−0.08	1.14	0.73	37	−2.67	4.25	−0.22
Atlantic	SDR v2.1	628	0.82	2.06	0.52	2895	1.30	3.18	0.42	26	−1.39	3.62	0.35
	SDR v3.0	805	0.17	1.18	0.57	3288	−0.72	1.82	0.49	22	−4.62	4.96	0.59
	CDR v1.1	687	0.09	1.08	0.56	2876	−0.91	1.64	0.63	21	−3.63	4.26	0.44
	NOAA v1.1	843	0.10	1.13	0.61	3449	−0.20	1.16	0.76	25	−1.32	2.67	0.44

v1.1 used ECMWF forecast winds) that were used to generate their respective GMF. In fact, their corresponding wind products are close to the real winds that include the stratification of the air near the surface. Thus, in this case we use actual buoy winds (stability included) for evaluating the newer three CYGNSS products.

3. Results

a. Direct comparison

In this section, comparisons among surface winds from CYGNSS products against the buoy winds are performed at both global and regional levels.

Figure 2 compares the aggregated collocated CYGNSS retrieved surface winds at the buoy locations. A close agreement between the retrieved winds and in situ wind measurements with the correlation coefficient ranging from ~0.7 (in SDR v2.1) to ~0.9 (in NOAA v1.1) is found. However, the collocated CYGNSS wind samples in SDR v2.1 and CDR v1.1, above ~12 m s^{-1}, are more widely dispersed, and the variability (standard deviation: SDR v2.1 = 2.84 m s^{-1}, CDR v1.1 = 2.24 m s^{-1}, SDR v3.0 = 2.33 m s^{-1}, NOAA v1.1 = 2.27 m s^{-1}) is greater relative to the SDR v3.0 and NOAA v1.1 products. The mean bias is 1.4 m s^{-1} for SDR v2.1, which is the largest among the datasets. In contrast, SDR v3.0, CDR v1.1, and NOAA v1.1 have smaller and negative mean biases (cf. Fig. 2: SDR v3.0 = −0.55 m s^{-1}, CDR v1.1 = −0.48 m s^{-1}, NOAA v1.1 = −0.1 m s^{-1}).

Among these datasets, the NOAA product exhibits smallest (−0.1 m s^{-1}) mean wind bias. In addition, the RMSD errors are found to be largest in the SDR v2.1 (3.08 m s^{-1}) and smallest in the NOAA v1.1 (1.21 m s^{-1}) wind products (Fig. 2). The variability in reference buoy winds for the matchup time periods is almost the same (see the standard deviation of the buoy winds). The RMSDs are about 127%, 66%, 71%, and 49% of the standard deviation of the buoy winds in SDR v2.1, CDR v1.1, SDR v3.0, and NOAA v1.1, respectively.

While the shapes of the wind histograms (see Fig. 3) are similar, discrepancies can clearly be seen, especially at the higher and lower wind speeds. The wind comparisons across the four products exhibit the greatest differences in SDR v2.1. In this, CYGNSS yields a relatively higher (lower) number of samples than the buoy measurements in the high (low) wind range. In contrast, the CDR v1.1 and SDR v3.0 show the opposite relation compared to SDR v2.1. The wind distributions between CYGNSS and buoys are quite consistent with NOAA v1.1.

Figure 4 shows the CYGNSS wind biases (CYGNSS–buoy) and RMSDs as a function of buoy wind speed. Note that the CYGNSS mission and the GNSS-R measurements approach in general are both fairly new. We assume the performance assessment by using buoy winds as the source of ground truth (illustrated by the *x* axis of Fig. 4) is more judicious than considering CYGNSS alone or mean of both buoy and CYGNSS winds at this position. The analyses of the dependence of the wind speed difference on the buoy winds show that the bias is small and positive for wind speeds below ~3 m s^{-1}, tends to zero in the buoy wind range of approximately 3–5 m s^{-1}, and is negative at higher wind speeds, approaching approximately −5 m s^{-1} (in CDR v1.1 and SDR v3.0) at speeds near 15 m s^{-1} (Fig. 4). At higher winds, the bias dependencies on buoy winds

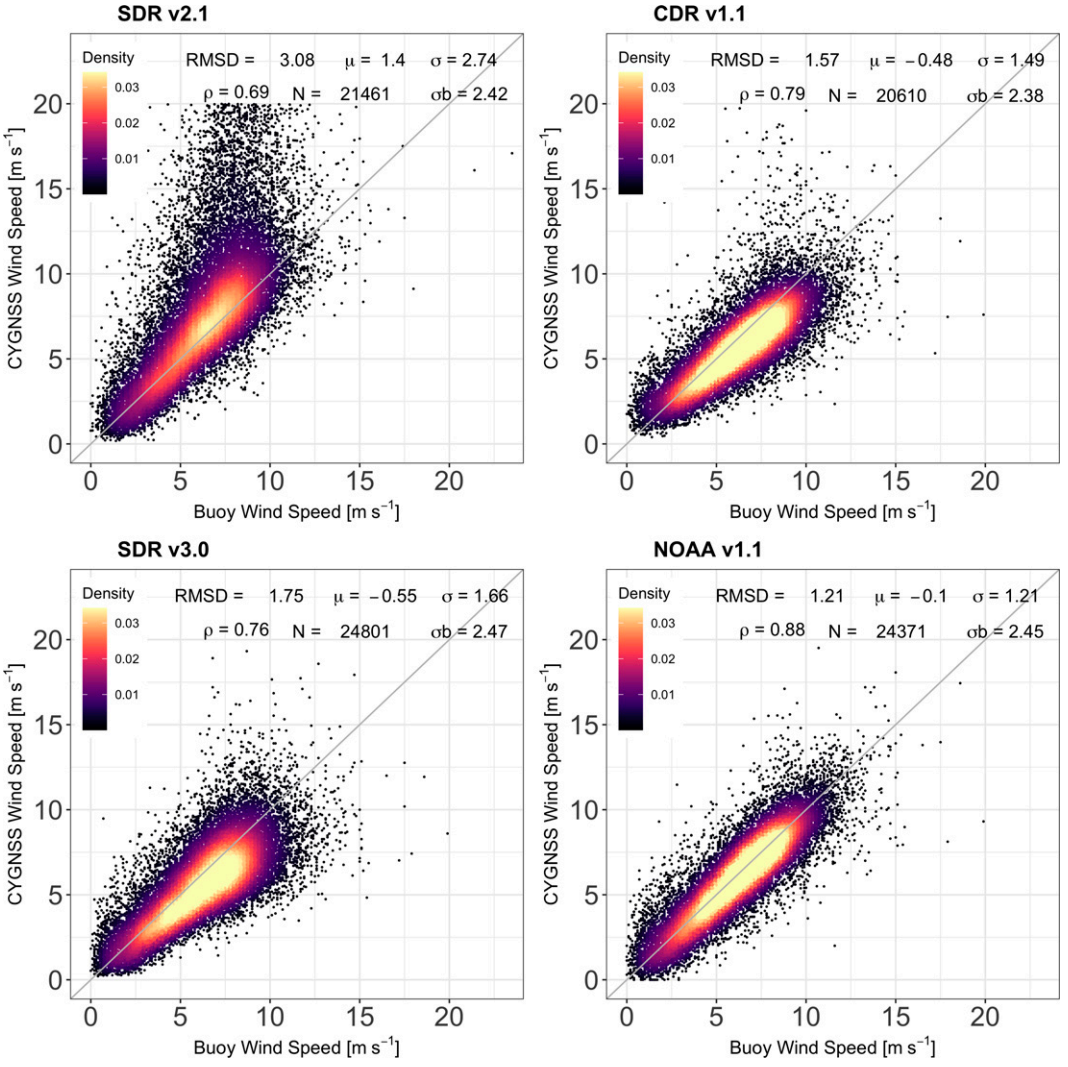

FIG. 2. A 2D density plot of collocated CYGNSS and tropical buoy wind speeds: (a) SDR v2.1, (b) CDR v1.1, (c) SDR v3.0, and (d) NOAA v1.1. The diagonal gray line is the 1:1 agreement. The statistical parameters RMSD, μ, σ, σb, and N are the root-mean-square difference, mean bias (CYGNSS − buoy), standard deviation of the difference (CYGNSS − buoy), standard deviation of buoy winds, and the total sample size of the collocated CYGNSS and buoy wind data, respectively. All CYGNSS data cover the period from 1 Aug 2018 to 28 Feb 2021.

show better performance for NOAA v1.1 and SDR v2.1 than the SDR v3.0 and CDR v1.1. The RMSD patterns changed and greatly increased for SDR v3.0 and CDR v1.1 compared to SDR v2.1 at the high wind range. The strong overestimation is mostly below 10 m s^{-1} due to large outliers found in the collocated SDR v2.1 data, whereas a slight underestimation (compared to the newer CYGNSS products) occurs above the 12 m s^{-1} wind speed. This can be seen in Fig. 4 and Table 1 (at the high wind range) more clearly. At the high wind range, the underestimation in CYGNSS winds generally found to be predominant. However, the outliers in CYGNSS SDR v2.1 data counterbalance the biases and thus improve the statistics compared to other wind products.

Since most of the collocation samples lie between 0 and ~14 m s^{-1} (see Fig. 4), the operational valid wind assessment, based on the CYGNSS L1 baseline requirement (Ruf et al. 2019b) can only be made for this range of wind speed at this point. In the case of NOAA v1.1 the RMSD curve intersects the 2 m s^{-1} uncertainty threshold at ~12.5 m s^{-1}, CDR v1.1 at ~9 m s^{-1}, and SDR v3.0 at ~8.5 m s^{-1}.

We further repeated our analyses for each of the three distinct tropical ocean basins, i.e., Indian, Atlantic, and Pacific. Figure 5 displays the 2D density scatterplot for each oceanic region. While the collocated data points mostly lie along the 1:1 line, the matchup density is found to be greatest in the low to moderate buoy wind range. However, the scatterplot shows a relatively more disperse relation in the Indian Ocean than Atlantic and Pacific Oceans. The RMSD value for CDR v1.1, SDR v3.0, NOAA v1.1 products tend to be higher in this region, where SDR v3.0 displays the greatest RMSD value

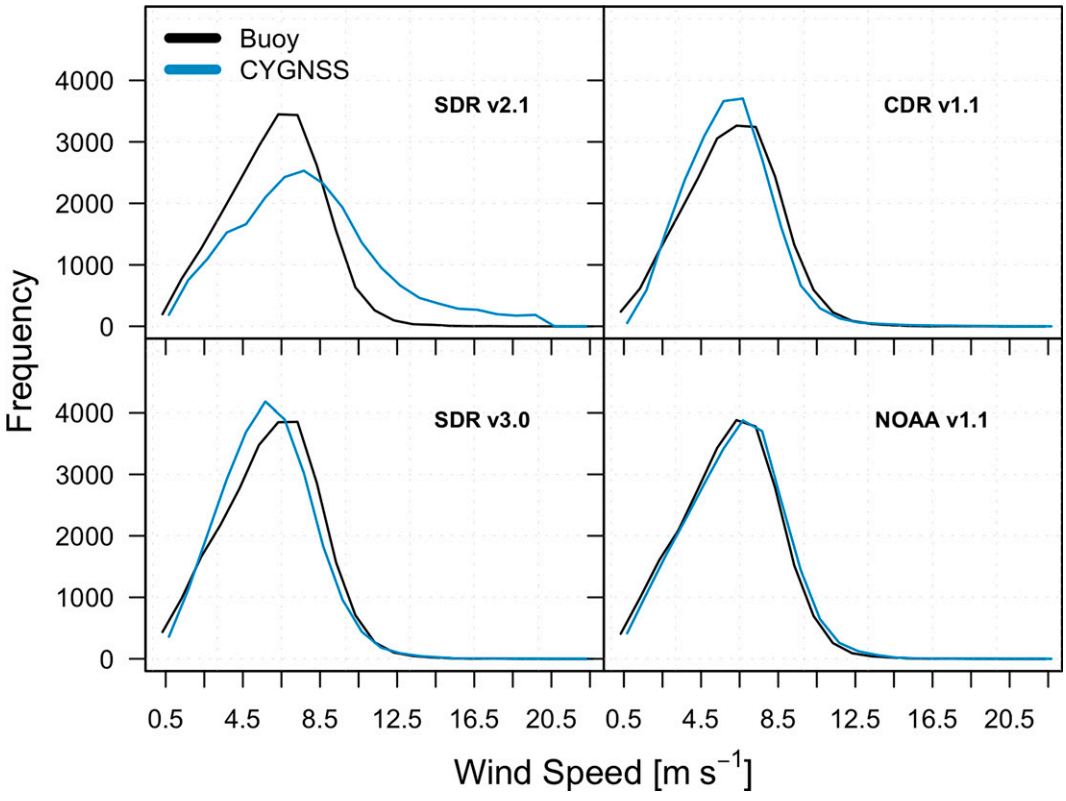

FIG. 3. Surface wind histograms (bin width: 1 m s^{-1}) for both CYGNSS and buoys.

(~1.84 m s^{-1} in the Indian Ocean). The smallest RMSD (~1.3 m s^{-1} in Indian Ocean) is found to be for the NOAA v1.1 wind product.

A great reduction in outliers, especially at the higher wind range, can be seen from SDR v2.1 to the CDR v1.1, SDR v3.0, and the NOAA v1.1 products (Fig. 5). The RMSD and bias values as a function of buoy winds for each oceanic region (not shown) show similar error patterns as above described for the globally aggregated stations analysis (Fig. 4), i.e., positive (negative) bias and larger RMSD in lower (higher) winds. However, at high winds, as shown in Table 1, the biases appear to be more pronounced and negative (~−3 to 5 m s^{-1}) for CDR v1.1 and SDR v3.0 than SDR v2.1 (~−0.5 to −1.4 m s^{-1}) and NOAA v1.1 (~−1.3 to −2.7 m s^{-1}). Large outliers can be seen in SDR v2.1 (Figs. 2 and 5); its relatively improved negative bias at high wind is due in part to compensating errors from these outliers. The NOAA wind product exhibits the smallest errors among the CYGNSS wind products, while SDR v2.1 exhibits the largest. With the exception of SDR v2.1, the wind speed histograms for the three oceans show similar shapes at the higher and lower wind speed ranges (Fig. 6). However, the Indian Ocean exhibits a slightly wider distribution than the other two oceans—indicating a pronounced number of low to moderate wind samples. The number of high winds (i.e., winds above 12 m s^{-1}) is also found to be greater in the Indian Ocean than in the Atlantic Ocean.

Figure 7 displays time series of monthly biases in all four CYGNSS winds for the Indian Ocean. The Indian Ocean is characterized by strong seasonal and interannual natural cycles, which can be inferred to some extent from the buoy monthly wind time series (Fig. 7). The region is, therefore, chosen specifically to examine whether the pronounced natural variabilities exist in CYGNSS wind biases, too. Note that the data length used (~4 years) may not be long enough to replicate well these natural signals.

Our analysis shows that the variations of periodic signals are evident in the bias time series of all CYGNSS wind products, though their magnitudes vary among the datasets. For example, SDR v2.1 tends to show strongest variation, whereas NOAA v1.1 indicates least variation in the wind bias. All data indicate a systematic underestimation (except SDR v2.1 in post June 2018) in comparison to buoy winds. Up to June 2018, the SDR v2.1, CDR v1.1, and NOAA winds are found to be ~5% less than buoy winds, whereas the standard deviations of these products are ~3 m s^{-1}, close to buoy data. It is interesting to note that the SDR v2.1 starts growing rapidly from February 2020 (Fig. 7). A possible explanation for this large difference is attributed to the fact that starting around this time, the flex power affected the transmit power of Block IIR-M GPS that majorly contributed to spurious fluctuation in σ_0, which ultimately resulted in a significant jump of the SDR v2.1 retrieved wind speed (Said et al. 2021). While the newer CYGNSS products do not show any trend, they show

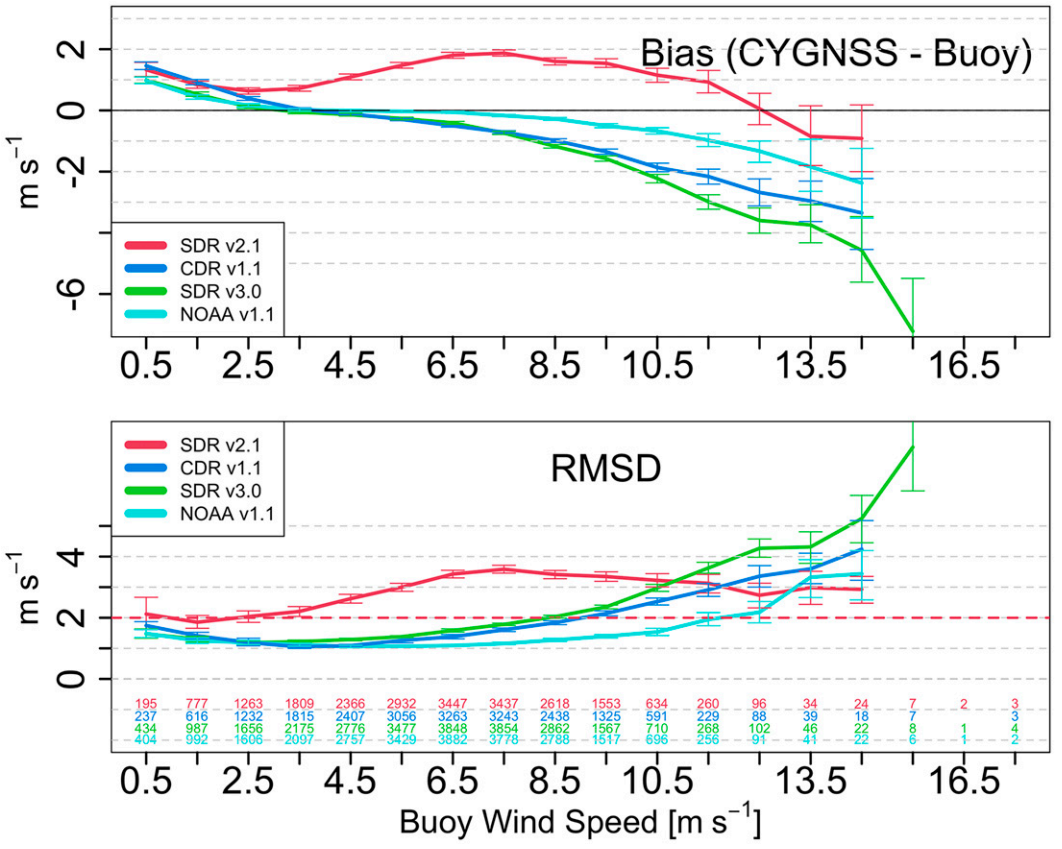

FIG. 4. RMS (blue line) and mean (red line; CYGNSS − buoy) difference between collocated buoy and CYGNSS wind speeds as a function of buoy wind speed: (a) wind bias (CYGNSS − buoy) and (b) RMSD. The solid error bars correspond to the 95% confidence limit, whereas the dashed error bars are the standard deviation. These metrics were computed over a ±0.5 m s^{-1} bin width for every 1 m s^{-1} buoy wind speed. Dashed horizontal red line in the bottom panel intersects the *y* axis at 2 m s^{-1}, indicating the CYGNSS mission baseline requirement for wind speed below 20 m s^{-1}. The sample size in each group of ±0.5 m s^{-1} bin width is marked by numeric text. All CYGNSS data cover the period from 1 Aug 2018 to 28 Feb 2021.

systematic negative biases throughout the period, which are found to be in the range of −0.5 to −1 m s^{-1}. The negative bias is more pronounced in SDR v3.0, whereas the offset between CDR v1.1 and NOAA v1.1 wind bias may partly be due to the different ancillary data products (i.e., MERRA-2 for CDR v1.1 and ECMWF/HWRF/IFREMER WaveWatch III forecast for NOAA v1.1) used by each of them to perform the trackwise correction. Figure 8 illustrates the RMSD and bias of wind estimates across the eight CYGNSS spacecraft (FM01 to FM08) for all four products. SDR v2.1 clearly shows a statistically significant positive bias in all spacecraft, while CDR v1.1 and SDR v3.0 show a negative bias. In contrast the biases in NOAA v1.1 are negligible. It is promising to see that the previously reported greatest outliers in FM01 and FM05 of SDR v2.1 are significantly suppressed in the newer CDR v1.1, SDR v3.0, and NOAA v1.1 products. The RMSDs in the NOAA product, which are generally below 1.5 m s^{-1}, are found to be smallest among the datasets.

b. *Performance in rain and convective systems*

All four CYGNSS wind products were further evaluated for various buoy measured hourly precipitation conditions. Here, we specifically performed an assessment for low wind (<6 m s^{-1}) cases only owing to the fact that rainfall appeared to have the largest effect on the CYGNSS low-wind estimates in our previous study (Asharaf et al. 2021). Figure 9a shows the RMSD values for four different rain conditions, i.e., heavy ($R > 1.0$ mm h^{-1}), moderate ($R > 0.2$ mm h^{-1}), negligible or scant ($R < 0.1$ mm h^{-1}), and nearly all rain conditions ($30 \leq R > 0$ mm h^{-1}). One can observe that the RMSDs are found to be significantly different from those in the full dataset when the rain rate is above 1.0 mm h^{-1}, relative to the scant or no rain ($R < 0.1$ m s^{-1}) case. The results are consistent with the previous finding of Asharaf et al. (2021). Among all CYGNSS products, the errors in SDR v2.1 are significantly higher than SDR v3.0 and NOAA products in conditions with heavy rain rates (>10 mm h^{-1}). Figure 9b shows the rain

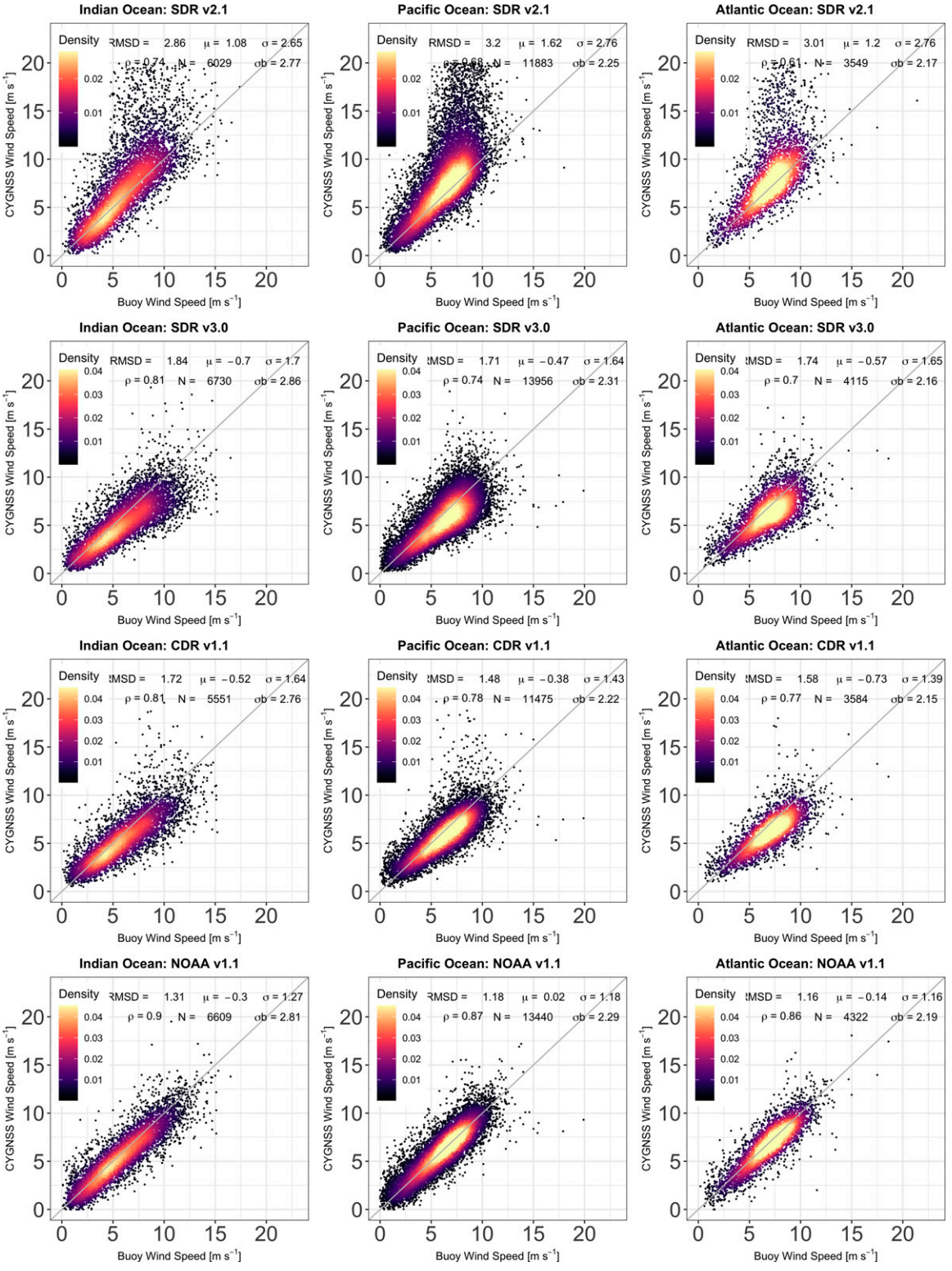

FIG. 5. As in Fig. 2, but for the (left) Indian, (center) Pacific, and (right) Atlantic Oceans.

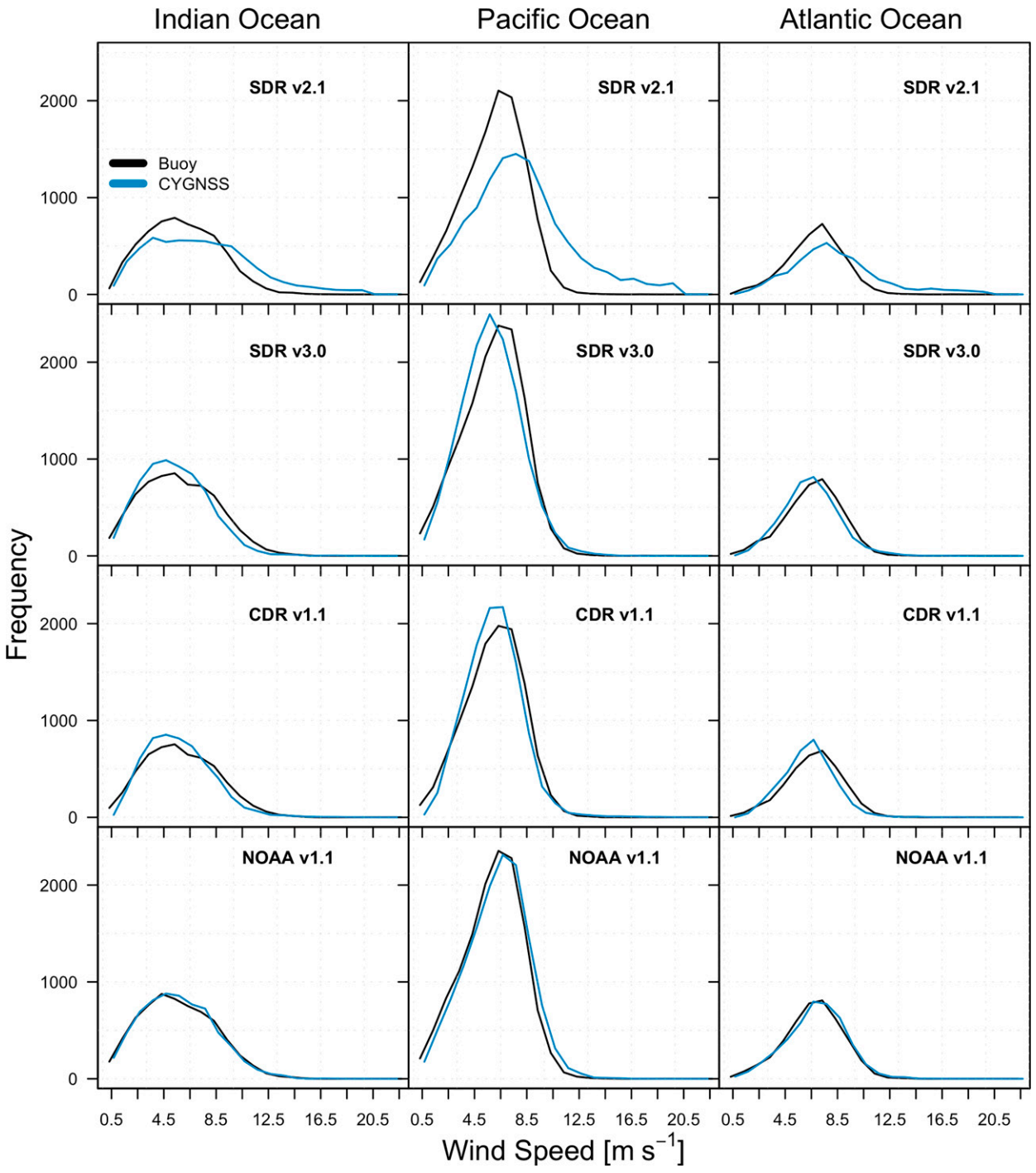

FIG. 6. Surface wind histograms (bin width: 1 m s^{-1}) for both CYGNSS and buoys for the (left) Indian, (center) Pacific, and (right) Atlantic Oceans. All CYGNSS data cover the period from 1 Aug 2018 to 28 Feb 2021.

effect on CYGNSS wind residuals computed from the buoy data. All CYGNSS products show a small positive bias that increases with increase in rain rate. However, the increasing slope and the correlation between the CYGNSS wind residuals and the buoy rain rate are found to be smaller for CDR v1.1, SDR v3.0, and NOAA v1.1 than for SDR v2.1.

Numerous studies have reported the existence of the intertropical convergence zone (ITCZ) in the tropics, which is an equatorial trough that exhibits a close connection with convection and its associated rainfall pattern (e.g., Waliser and Jiang 2015). The structure and movement of the ITCZ over a range of latitudes play an important role in characterizing

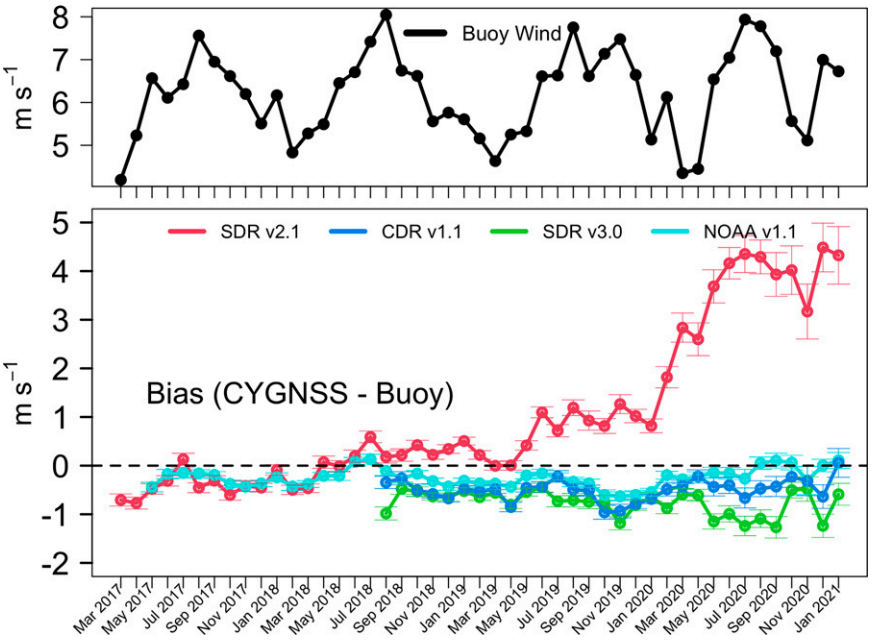

FIG. 7. Monthly time series of the collocated (top) buoy mean wind speed and (bottom) bias for the Indian Ocean. SDR v2.1 and NOAA v1.1 data start from 18 Mar and 1 May 2017, respectively. The error bars correspond to the 95% confidence limit.

the strength of ocean–atmosphere interaction. Given the importance of the ITCZ in the tropics, it is worth investigating how likely it is that the retrieved CYGNSS winds will change in convective regions, and how the results will vary among the CYGNSS products. To do so, we conducted a wind speed comparison using the buoy datasets over the ITCZ region in the tropical Pacific Ocean. For this particular analysis, the ITCZ region is defined by the Integrated Multisatellite Retrievals for GPM (IMERG; Huffman et al. 2019) gridded precipitation data, covering the longitude range 150°–110°W.

The analysis indicates a tendency of positive wind bias and higher RMSD over the ITCZ region (cf. Fig. 10), while the differences are least and insignificant outside the region. The increased biases and RMSDs follow closely the seasonal evolution of the ITCZ band. To make it more visible, we extended the analysis by averaging across the aforementioned longitude and plot the mean bias and RMSD along the geographical latitude for all four products (Fig. 11). We also added the IMERG rainfall and buoy measured wind speed to illustrate explicitly the latitudinal migration of the ITCZ event. It shows that all CYGNSS winds tend to yield higher error (both in bias and RMSD) in the ITCZ band, covering from 2° to 11°N latitude. The errors are remarkably high in SDR v2.1; however, it is interesting to see that the RMSDs are found to be significantly suppressed in the remaining CYGNSS products (the wind difference from SDR v2.1 is ~1.5 to 1.0 m s^{-1} in CDR v1.1 and SDR v3.0 versus ~2.5 m s^{-1} in NOAA v1.1 winds). Prior to August 2018, the SDR v2.1 product follows nearly the same error pattern as the newer CYGNSS products, yet a relatively large deviation in all data products is found over the ITCZ band (Fig. 11, see the dotted red line in the bias and RMSD plots). Similar error characteristics in all CYGNSS winds were also found in the ITCZ over the Atlantic Ocean (not shown).

4. Discussion

The difference between the retrieved and buoy winds are found to be in general consistent (with the exception being SDR v2.1); however, the discrepancies are notable at the higher and lower wind ranges in all four CYGNSS products. The differences at the higher winds can be attributed to the backscattered signal attenuation problem and the CYGNSS calibration issue. For instance, Ruf et al. (2019a) suggested that the decrease in sensitivity of the GMF with increasing wind speeds is one of the major factors responsible for the error growth in high winds.

While the wind speed estimates from CYGNSS are generally consistent with the buoy observations, the Indian Ocean exhibits a slightly larger error than in the Pacific and Atlantic Oceans. As supported by scatterplot (Fig. 5) and histogram (Fig. 6), the Indian Ocean has more collocated samples (~59%–65%) than the Atlantic Ocean, and yet it does not show such high-density cluster on the scatterplot as found in the Pacific and Atlantic Oceans, indicating the wind speed estimates have more variability (cf. the relatively wider wind distribution plot in Fig. 6) for the Indian Ocean than the other two seas.

In the tropics, over the Indian and western Pacific Oceans, large- or planetary-scale intraseasonal oscillations predominantly occur. For instance, one important mode of intraseasonal

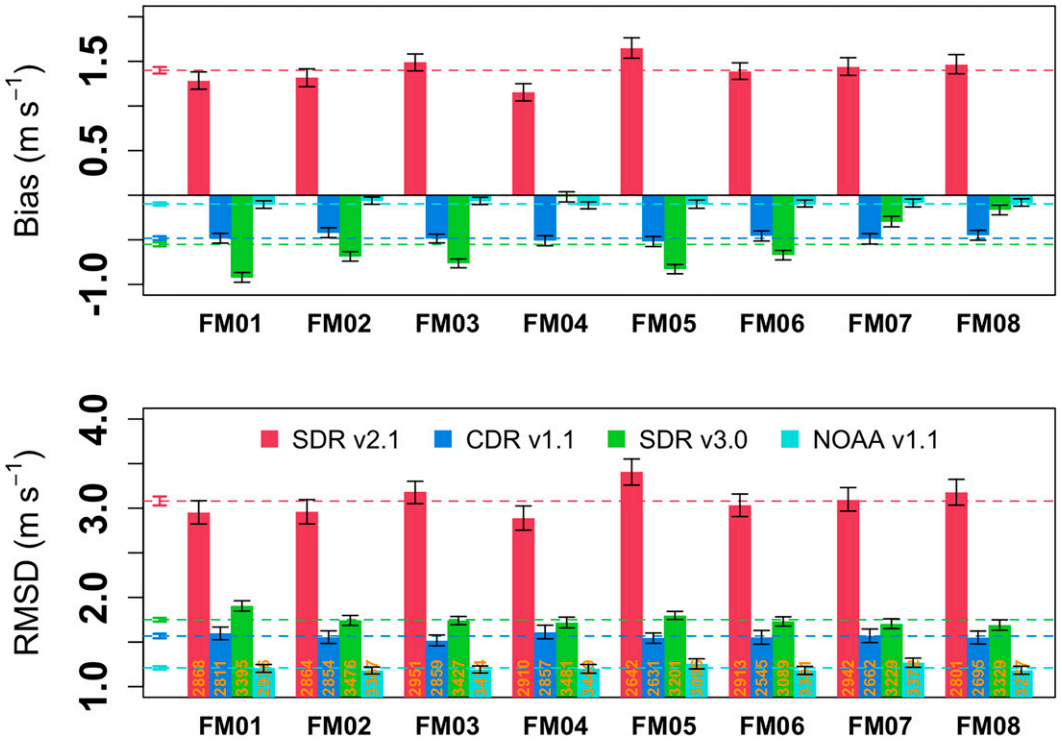

FIG. 8. (top) Bias and (bottom) RMSD between CYGNSS and buoy winds in each CYGNSS spacecraft (FM01 to FM08). Sample size is given by numbers on each bar in the bottom panel. Horizontal dashed lines are the combined spacecraft (top) bias and (bottom) RMSD values, whereas the error bars represent the 95% confidence interval estimated by the bootstrapping (random sampling of 1000 times with replacement) approach. All CYGNSS data are on a common time period, as listed in Table 1.

variability is the Madden–Julian oscillation (MJO), which leads to higher wind speed variability and can significantly influence precipitation processes. Moreover, the climatology of the diurnal signals, especially over the Indian and west Pacific Oceans is stronger and more tightly coupled with heavy rainfall and deep convection than in the other regions (Yang and Slingo 2001). The increased convection and variability in the planetary-scale processes in the Indian Ocean may contribute to increasing the roughness of the sea surface, thereby increasing the susceptibility to the error growth in the CYGNSS wind speeds. Because the wind speeds observed by CYGNSS are sensitive to rain at low wind speeds ($<\sim$6 m s^{-1}) and the lower wind speeds are observed in the Indian and west Pacific Oceans, it is likely that additional errors are introduced in CYGNSS over these regions. The apparent differences in the present analysis can also be explained by the fact that the collocated sample size of higher wind speeds is also greater in the Indian compared to the Atlantic Ocean (see the wind distribution in Fig. 6 and Table 1). Moreover, CYGNSS has a known bias at higher wind speeds, as indicated above (Fig. 3) and in previous studies (Ruf et al. 2019a,b). This may lead to further uncertainties in the CYGNSS derived wind speeds in this regime.

In the present study, the inconsistencies, especially in CYGNSS SDR v2.1, occur, as shown in Fig. 7, after July 2018. The CDR v1.1 product does not show any spurious increasing trend in the monthly bias time series, thanks in part to the use of better calibrated NBRCS and the implemented trackwise NBRCS correction. The SDR v2.1 algorithm assumes GPS behavior does not vary with time, whereas the latest CYGNSS products use time dependent corrections. It has been noticed that the large changes in SDR v2.1 occurred when GPS changes its flex power operating mode mostly after February 2020 (Said et al. 2021). The CYGNSS products also include a ~60-day periodicity, which is the period of the CYGNSS orbit plane beta angle precession, and also the period of long-term variations in the physical temperature of the CYGNSS receivers.

It was found in previous studies (Asharaf et al. 2021; Asgarimehr et al. 2018) that rain splashing effects on ocean surface roughness, and by extension, scatterometer estimates of wind, are noteworthy at low wind speeds. Our present analyses are consistent with these previous findings, indicating rain effects on the CYGNSS wind residuals are minor, and occur at low wind speeds for all four CYGNSS products. Similar to Fig. 9, we have repeated the rain dependency analysis by using the IMERG rainfall data product. Despite the different spatial scales in the rainfall dataset (e.g., buoy at point scale and IMERG at 0.1°), both data products show nearly identical results, albeit the sample size is found to be relatively higher with the gridded IMERG dataset (Fig. S1 in the online supplemental material). The increasing positive bias trend under low wind conditions can be associated with the current

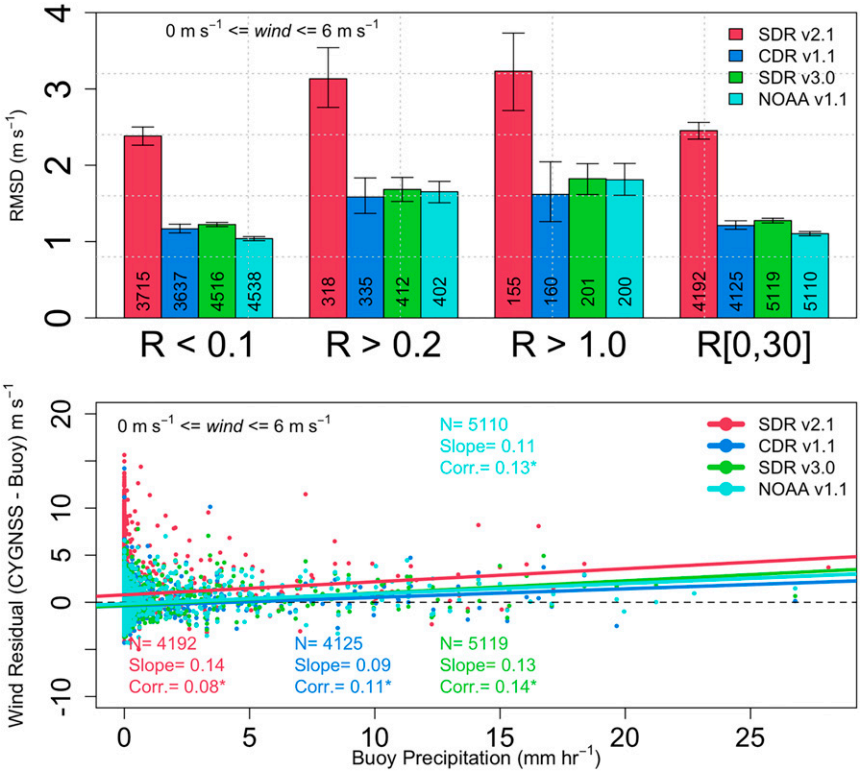

FIG. 9. (top) RMSD (indicated by bars) and (bottom) scatterplot of CYGNSS winds at the analyzed buoys (negative means buoy values are higher) as functions of buoy precipitation rate at different rain (R in mm h^{-1}) conditions. The best-fit linear regression lines onto the scatterplots are shown in (b). The error bars correspond to the 95% confidence limit estimated via the bootstrap method. Matchup samples are illustrated by number.

level-1 calibration issue that does not apply a correction for rain induced attenuation (Balasubramaniam and Ruf 2018).

The slightly degraded performance of the CYGNSS wind products over the ITCZ region can partly be linked to the occurrence of multiscale convection and convective variability in the region. It is observed that the improvement in bias and RMSD over the ITCZ region are greater in the NOAA v1.1. and CDR v1.1 wind products due to the trackwise correction algorithm applied with both the products. However, the correction algorithm is largely dependent on the used ancillary numerical model wind data that can inherently affect the track wise correction performance (Said et al. 2021), since the quality of numerical model wind data heavily relies on the model parameterization schemes, especially over the convective region. It must be emphasized here that the ITCZ is a large-scale feature, whereas each buoy measurement is representative of a point—or at best a very limited local region. Fine-scale processes that affect winds measured by a buoy might not be adequately represented by CYGNSS winds over a 25 km footprint. Indeed, CYGNSS may better represent the ITCZ large-scale processes due to a larger CYGNSS footprint size relative to the buoy point measurement. Aside from considerations regarding the spatial scale of the measurements, the wind speeds observed by CYGNSS are sensitive to rain at low wind speeds ($<\sim 6$ m s^{-1}) and lower wind speeds and heavy rainfall are associated with the ITCZ band. Moreover, the diurnal uncertainties could also be one of the crucial contributing factors involved in the CYGNSS wind speed errors over the region. To examine this effect, we have selected a set of buoys along latitudes that follow the 125°W longitude line, and then the RMSD and bias are computed at the diurnal local standard time every 3 h (Fig. S2). The statistics indicate that the errors in CYGNSS winds are somewhat increased in the ITCZ band. The differences are also found in the early morning and afternoon time where the atmosphere is considered to be relatively more stable and unstable, respectively. Thus, these all may add another level of complexity to the CYGNSS wind retrieval and correction process for the regions with widespread intense convection.

5. Conclusions

The present study gives an update on the performance of four available CYGNSS wind products against high-quality tropical buoy arrays. All four products tend to be in close agreement and show similar error characteristics at high and low wind speeds. For example, CYGNSS wind speed underestimates at the higher buoy winds and overestimates lower

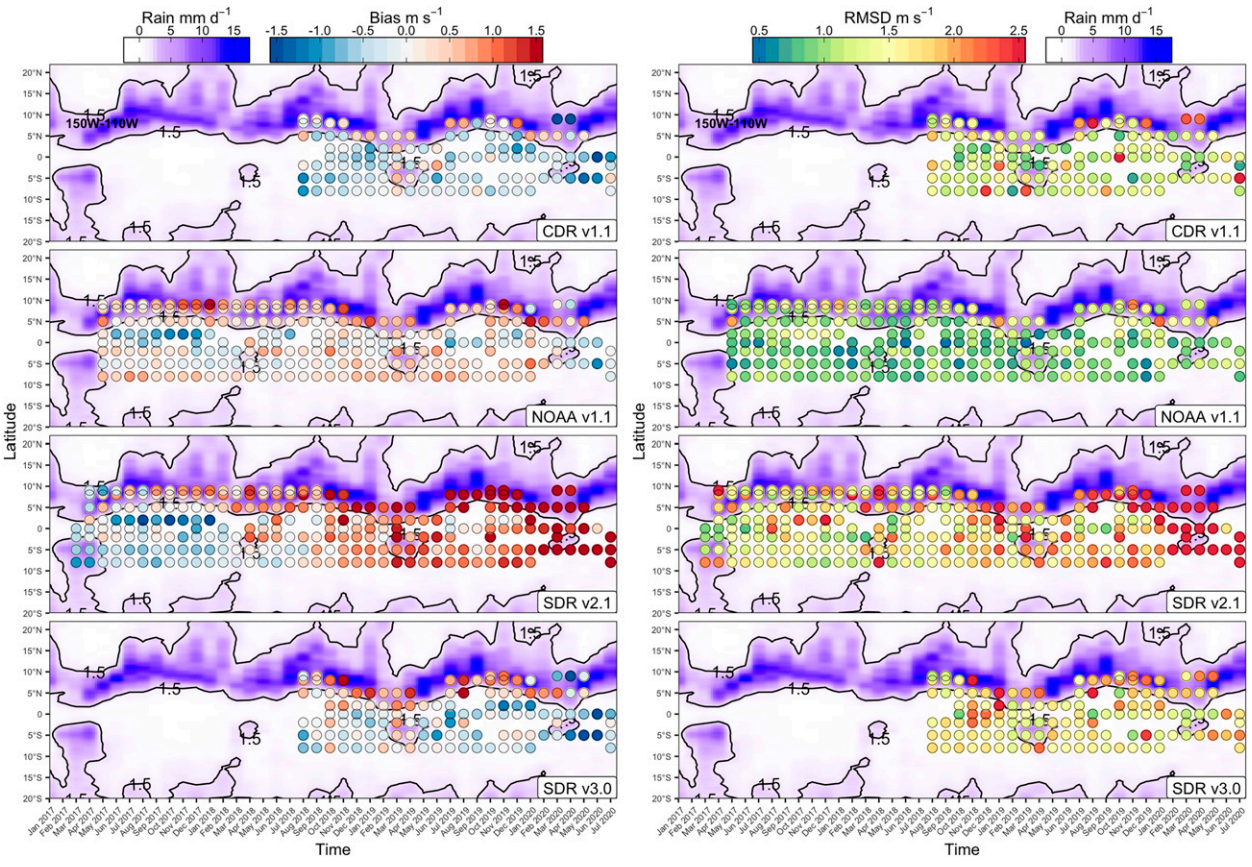

FIG. 10. Hovmöller diagram for the (left) mean bias and (right) RMSD between CYGNSS and buoys winds. The longitudinal average was taken over 150°–110°W. GPM (IMERG) rainfalls, indicating the ITCZ convective bands, are shown by blue shading and black contour lines.

buoy winds. However, the winds in SDR v2.1 appear to have a drift in bias that begins in July 2018. The trackwise correction and updated GMFs significantly improve the retrieved winds, which can be observed in the decrease in scatterplot variability for the CDR v1.1, and NOAA datasets, relative to SDR v2.1. The aggregated wind matchup statistics suggest that the improvement in RMSDs is about 49% for CDR v1.1, 43% for SDR v3.0, and 61% for NOAA v1.1 product when compared to the CYGNSS SDR v2.1 winds. In addition, the outliers found for specific CYGNSS spacecraft (FM01 and FM05) in the SDR v2.1 dataset are significantly reduced in the updated CYGNSS data releases.

While the CYGNSS products have slight rain dependency in light wind conditions, the relative performance among the CYGNSS datasets show promising results for CDR v1.1, SDR v3.0, and NOAA v1.1 compared to SDR v2.1 retrieved winds. The improvement can also be seen along the ITCZ band, where all products are shown to have relatively larger bias and RMSD values than outside the convective band.

The present comparison statistics overall indicate that the agreement between newly retrieved winds from the CYGNSS mission and tropical buoys is within the 2 m s^{-1} threshold defined by NASA level-1 science mission requirements. This requirement is consistent with the previous finding of Ruf et al. (2019b) and Asharaf et al. (2021). Although the latest CYGNSS products (CDR v1.1 and NOAA v1.1) use the trackwise correction algorithm that removes the physical temperature dependent bias of the CYGNSS receivers, there are still residual errors in the temperature dependent corrections in the L1 calibration algorithm.

The near-term consideration is to improve the SDR v3.0 and CDR v1.1 CYGNSS L2 winds by addressing this issue and also incorporating the significant wave height information to the wind speed retrieval algorithm, similar to NOAA v1.1 [see Said et al. (2021) for more details]. Note that the significant wave height is sensitive to the longer wavelength parts of the roughness spectrum, and therefore using it in the retrieval algorithm provides a means to correct for signals in the CYGNSS data that are not due to locally wind generated waves. Of course, significant wave height is also sensitive to local wind speed, so there is the possibility that information about the local wind may be included in the model which provides the significant wave height data. This possibility was recently addressed in Pascual et al. (2021), and was found not to be a significant contributing factor. The improvements to L1 calibration planned for SDR v3.1 are described in Gleason et al. (2022). The improvements to L2 wind speed

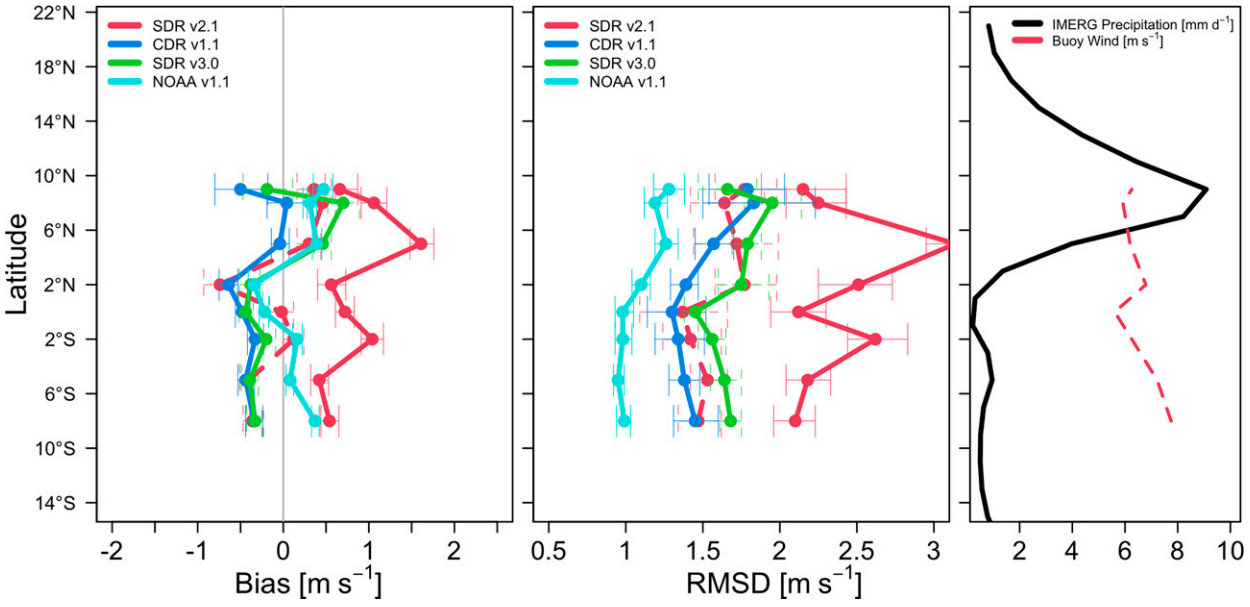

FIG. 11. As in Fig. 10, except the averaging was performed over both time and longitude (150°–110°W). The error bars correspond to the 95% confidence limit estimated via the bootstrap method. (right) The GPM (IMERG) rainfall and buoy winds. SDR v2.1 (March 2017–July 2018) is shown by a red dashed line in the RMSD and bias plots.

retrieval planned for SDR v3.1 are described in Pascual et al. (2021). Initial results with these new algorithms are encouraging and are found to improve the CYGNSS wind performance at high wind speeds.

Acknowledgments. The authors acknowledge Jet Propulsion Laboratory (JPL) for providing computational resources. SA express his sincere thanks to NOAA/PMEL group for the buoy data support. DJP's contributions to this study were carried out on behalf of the Jet Propulsion Laboratory, California Institute of Technology, under a contract with the National Aeronautics and Space Administration. CSR's contributions were supported in part by NASA Science Mission Directorate Contract NNL13AQ00C with the University of Michigan. Finally, we thank the anonymous reviewers for their constructive comments and suggestions that significantly improved the quality of this manuscript.

Data availability statement. All CYGNSS level-2 wind products used during this study are openly available from the NASA PO.DAAC server at https://podaac.jpl.nasa.gov/CYGNSS. The GPM IMERG Final Precipitation level-3 (0.1° × 0.1°), v06, data are available at the Goddard Earth Sciences Data and Information Services Center (GES DISC; 10.5067/GPM/IMERG/3B-MONTH/06). Tropical buoys (TAO/TRITAN/PIRATA) data can be obtained by using the FTP client at https://www.pmel.noaa.gov/tao/drupal/disdel/.

REFERENCES

Alpers, W., and B. Brümmer, 1994: Atmospheric boundary layer rolls observed by the synthetic aperture radar aboard the ERS-1 satellite. *J. Geophys. Res.*, **99**, 12 613–12 621, https://doi.org/10.1029/94JC00421.

Asgarimehr, M., V. Zavorotny, J. Wickert, and S. Reich, 2018: Can GNSS reflectometry detect precipitation over oceans? *Geophys. Res. Lett.*, **45**, 12 585–12 592, https://doi.org/10.1029/2018GL079708.

Asharaf, S., D. E. Waliser, D. J. Posselt, C. S. Ruf, C. Zhang, and A. W. Putra, 2021: CYGNSS ocean surface wind validation in the tropics. *J. Atmos. Oceanic Technol.*, **38**, 711–724, https://doi.org/10.1175/JTECH-D-20-0079.1.

Balasubramaniam, R., and C. S. Ruf, 2018: Improved calibration of CYGNSS measurements for downbursts in the intertropical convergence zone. *2018 IEEE Int. Geosciences and Remote Sensing Symp.*, Valencia, Spain, IEEE, 3987–3990, https://doi.org/10.1109/IGARSS.2018.8517571.

Bhate, J., A. Munsi, A. Kesarkar, G. Kutty, and S. K. Deb, 2021: Impact of assimilation of satellite retrieved ocean surface winds on the tropical cyclone simulations over the north Indian Ocean. *Earth Space Sci.*, **8**, e2020EA001517, https://doi.org/10.1029/2020EA001517.

Bourlès, B., and Coauthors, 2008: The PIRATA program: History, accomplishments, and future directions. *Bull. Amer. Meteor. Soc.*, **89**, 1111–1126, https://doi.org/10.1175/2008BAMS2462.1.

Boutin, J., and J. Etcheto, 1990: Seasat scatterometer versus scanning multichannel microwave radiometer wind speeds: A comparison on a global scale. *J. Geophys. Res.*, **95**, 22 275–22 288, https://doi.org/10.1029/JC095iC12p22275.

Chelton, D. B., and M. H. Freilich, 2005: Scatterometer-based assessment of 10-m wind analyses from the operational ECMWF and NCEP numerical weather prediction models. *Mon. Wea. Rev.*, **133**, 409–429, https://doi.org/10.1175/MWR-2861.1.

Clarizia, M. P., and C. S. Ruf, 2016: Wind speed retrieval algorithm for the Cyclone Global Navigation Satellite System (CYGNSS) mission. *IEEE Trans. Geosci. Remote Sens.*, **54**, 4419–4432, https://doi.org/10.1109/TGRS.2016.2541343.

——, V. Zavarotny, and C. S. Ruf, 2018: Level 2 wind speed retrieval. CYGNSS Algorithm Theoretical Basis Doc., 101 pp.

CYGNSS, 2018: CYGNSS level 2 science data record, version 2.1. PO.DAAC, accessed 20 September 2018, https://doi.org/10.5067/CYGNS-L2X21.

——, 2020: CYGNSS level 2 science data record, version 3.0. PO.DAAC, accessed 26 January 2021, https://doi.org/10.5067/CYGNS-L2X30.

——, 2021: CYGNSS level 2 climate data record, version 1.1. PO.DAAC, accessed 14 January 2021, https://doi.org/10.5067/CYGNS-L2C11.

Edson, J. B., and Coauthors, 2013: On the exchange of momentum over the open ocean. *J. Phys. Oceanogr.*, **43**, 1589–1610, https://doi.org/10.1175/JPO-D-12-0173.1.

Fairall, C. W., E. F. Bradley, J. E. Hare, A. A. Grachev, and J. B. Edson, 2003: Bulk parameterization of air–sea fluxes: Updates and verification for the COARE algorithm. *J. Climate*, **16**, 571–591, https://doi.org/10.1175/1520-0442(2003)016<0571:BPOASF>2.0.CO;2.

Gelaro, R., and Coauthors, 2017: The Modern-Era Retrospective Analysis for Research and Applications, version 2 (MERRA-2). *J. Climate*, **30**, 5419–5454, https://doi.org/10.1175/JCLI-D-16-0758.1.

Gleason, S., M. M. Al-Khaldi, C. S. Ruf, D. S. McKague, T. Wang, and A. Russel, 2022: Characterizing and mitigating digital sampling effects on the CYGNSS level 1 calibration. *IEEE Trans. Geosci. Remote Sens.*, **60**, 1–12, https://doi.org/10.1109/TGRS.2021.3120026.

Hersbach, H., and Coauthors, 2020: The ERA5 global reanalysis. *Quart. J. Roy. Meteor. Soc.*, **146**, 1999–2049, https://doi.org/10.1002/qj.3803.

Huffman, G. J., E. F. Stocker, D. T. Bolvin, E. J. Nelkin, and J. Tan, 2019: GPM IMERG final precipitation L3 half hourly 0.1 degree × 0.1 degree, version 06. GES DISC, accessed 1 January 2018, https://doi.org/10.5067/GPM/IMERG/3B-HH/06.

Kobayashi, S., and Coauthors, 2015: The JRA-55 Reanalysis: General specifications and basic characteristics. *J. Meteor. Soc. Japan*, **93**, 5–48, https://doi.org/10.2151/jmsj.2015-001.

Li, X., J. R. Mecikalski, and T. J. Lang, 2020: A study on assimilation of CYGNSS wind speed data for tropical convection during 2018 January MJO. *Remote Sens.*, **12**, 1243, https://doi.org/10.3390/rs12081243.

Liu, W. T., 1984: The effects of the variations in sea surface temperature and atmospheric stability in the estimation of average wind speed by SEASAT-SASS. *J. Phys. Oceanogr.*, **14**, 392–401, https://doi.org/10.1175/1520-0485(1984)014<0392:TEOTVI>2.0.CO;2.

May, J. C., and M. A. Bourassa, 2011: Quantifying variance due to temporal and spatial difference between ship and satellite winds. *J. Geophys. Res.*, **116**, C08013, https://doi.org/10.1029/2010JC006931.

McPhaden, M. J., and Coauthors, 1998: The Tropical Ocean-Global Atmosphere (TOGA) observing system: A decade of progress. *J. Geophys. Res.*, **103**, 14 169–14 240, https://doi.org/10.1029/97JC02906.

——, and Coauthors, 2009: RAMA: The Research Moored Array for African–Asian–Australian Monsoon Analysis and Prediction. *Bull. Amer. Meteor. Soc.*, **90**, 459–480, https://doi.org/10.1175/2008BAMS2608.1.

Pascual, D., M. P. Clarizia, and C. S. Ruf, 2021: Improved CYGNSS wind speed retrieval using significant wave height correction. *Remote Sens.*, **13**, 4313, https://doi.org/10.3390/rs13214313.

Rennie, M. P., and L. Isaksen, 2020: The NWP impact of Aeolus level-2B winds at ECMWF. ECMWF Tech. Memo. 864, 110 pp., https://doi.org/10.21957/alift7mhr.

——, ——, F. Weiler, J. de Kloe, T. Kanitz, and O. Reitebuch, 2021: The impact of Aeolus wind retrievals in ECMWF global weather forecasts. *Quart. J. Roy. Meteor. Soc.*, **147**, 3555–3586, https://doi.org/10.1002/qj.4142.

Ruf, C., and Coauthors, 2016: CYGNSS handbook. University of Michigan Doc., 155 pp.

——, and R. Balasubramaniam, 2019: Development of the CYGNSS geophysical model function for wind speed. *IEEE J. Sel. Top. Appl. Earth Obs. Remote Sens.*, **12**, 66–77, https://doi.org/10.1109/JSTARS.2018.2833075.

——, S. Gleason, and D. S. McKague, 2019a: Assessment of CYGNSS wind speed retrieval uncertainty. *IEEE J. Sel. Top. Appl. Earth Obs. Remote Sens.*, **12**, 87–97, https://doi.org/10.1109/JSTARS.2018.2825948.

——, S. Asharaf, R. Balasubramaniam, S. Gleason, T. Lang, D. McKague, D. Twigg, and D. E. Waliser, 2019b: In-orbit performance of the constellation of CYGNSS hurricane satellites. *Bull. Amer. Meteor. Soc.*, **100**, 2009–2023, https://doi.org/10.1175/BAMS-D-18-0337.1.

Saha, S., and Coauthors, 2014: The NCEP Climate Forecast System version 2. *J. Climate*, **27**, 2185–2208, https://doi.org/10.1175/JCLI-D-12-00823.1.

Said, F., Z. Jelenak, J. Park, S. Soisuvarn, and P. S. Chang, 2019: A 'track-wise' wind retrieval algorithm for the CYGNSS mission. *2019 IEEE Int. Geoscience and Remote Sensing Symp.*, Yokohama, Japan, IEEE, 8711–8714, https://doi.org/10.1109/IGARSS.2019.8898099.

——, ——, ——, and P. S. Chang, 2021: The NOAA track-wise wind retrieval algorithm and product assessment for CYGNSS. *IEEE Trans. Geosci. Remote Sens.*, **60**, 4202524, https://doi.org/10.1109/TGRS.2021.3087426.

Short, E., C. L. Vincent, and T. P. Lane, 2019: Diurnal cycle of surface winds in the Maritime Continent observed through satellite scatterometry. *Mon. Wea. Rev.*, **147**, 2023–2044, https://doi.org/10.1175/MWR-D-18-0433.1.

SOCD, 2020: NOAA CYGNSS level 2 science wind speed 25-km product, version 1.1. PO.DAAC, accessed 4 October 2020, https://doi.org/10.5067/CYGNN-22511.

Waliser, D. E., and X. Jiang, 2015: Tropical meteorology: Intertropical convergence zones (ITCZ). *Encyclopedia of Atmospheric Sciences*. 2nd ed. Vol. 6, Academic Press, 121–131.

Wang, T., C. S. Ruf, B. Block, D. S. McKague, and S. Gleason, 2019: Design and performance of a GPS constellation power monitor system for improved CYGNSS L1B calibration. *IEEE J. Sel. Top. Appl. Earth Obs. Remote Sens.*, **12**, 26–36, https://doi.org/10.1109/JSTARS.2018.2867773.

Yang, G.-Y., and J. Slingo, 2001: The diurnal cycle in the tropics. *Mon. Wea. Rev.*, **129**, 784–801, https://doi.org/10.1175/1520-0493(2001)129<0784:TDCITT>2.0.CO;2.

Zavorotny, V. U., and A. G. Voronovich, 2000: Scattering of GPS signals from the ocean with wind remote sensing application. *IEEE Trans. Geosci. Remote Sens.*, **38**, 951–964, https://doi.org/10.1109/36.841977.